

# Soft Matter

Accepted Manuscript



This is an *Accepted Manuscript*, which has been through the Royal Society of Chemistry peer review process and has been accepted for publication.

*Accepted Manuscripts* are published online shortly after acceptance, before technical editing, formatting and proof reading. Using this free service, authors can make their results available to the community, in citable form, before we publish the edited article. We will replace this *Accepted Manuscript* with the edited and formatted *Advance Article* as soon as it is available.

You can find more information about *Accepted Manuscripts* in the [Information for Authors](#).

Please note that technical editing may introduce minor changes to the text and/or graphics, which may alter content. The journal's standard [Terms & Conditions](#) and the [Ethical guidelines](#) still apply. In no event shall the Royal Society of Chemistry be held responsible for any errors or omissions in this *Accepted Manuscript* or any consequences arising from the use of any information it contains.

# Rheology Modulated Contact Line Dynamics of an Immiscible Binary System under Electrical Double Layer Phenomena

*Pranab Kumar Mondal<sup>1,2</sup>, Debabrata DasGupta<sup>1</sup>, and Suman Chakraborty<sup>1,2</sup>*

<sup>1</sup>*Department of Mechanical Engineering, Indian Institute of Technology Kharagpur, West Bengal, India - 721302*

<sup>2</sup>*Advanced Technology Development Center, Indian Institute of Technology Kharagpur, West Bengal, India- 721302*

Soft Matter Accepted Manuscript

---

Email address: [suman@mech.iitkgp.ernet.in](mailto:suman@mech.iitkgp.ernet.in)

**Abstract**

We investigate electrically driven contact line dynamics of a binary fluid system constituted by one Newtonian and other non-Newtonian fluid in a narrow fluidic channel with chemically patched walls. We use power-law model to describe the rheology of the non-Newtonian fluid and diffuse interface phase-field method to model dynamics of multiple phases. We bring out the alteration in the interfacial dynamics as attributable to the rheology driven modifications in the interfacial stress and its interplay with the Maxwell stress originating from electrokinetic effects.

## I. Introduction

When two immiscible fluids are in contact with a solid surface, the dynamics of the contact line formed at the fluid-fluid-solid interface plays an important role, and leads to far ranging consequences across scales.<sup>1-13</sup> It is, therefore, not a surprising fact to appreciate the deep involvement of researchers from various disciplines on the systematic interrogation of the underlying physics associated with the contact line motion of immiscible binary fluid systems.<sup>14-17</sup> Coupled with other aspects of chemical physics over interfacial scales<sup>18-21</sup> a thorough understanding of the contact line dynamics of binary fluid systems has led to significant advancements in the design and development of several miniaturized devices of modern day technological relevance.<sup>5,7,22-30</sup> In many of these devices, use of electrical actuation is a common practice now-a-days, primarily attributable to a possible elimination of moving parts and the on-chip integrability of the fluidic system under concern. Recognizing this aspect, several researchers have addressed the underlying dynamics of electrically actuated two phase flows in different applications.<sup>31-39</sup> However, they have mostly considered the driving and driven fluids to be Newtonian in binary flow configurations.

Recent advancements in lab-on-a-chip based micro-total-analysis systems, such as those commonly used for on-chip bio analysis, transportation of bio-fluids etc., have triggered the needs of understanding the interfacial dynamics of a binary fluid system in a miniaturized environment in which one of the fluids is non Newtonian in nature. The working fluids in these devices belong to the broad class of soft binary system. Typical examples concern blood (which is a typical shear-thinning fluid) samples being handled in microfluidics based pathological diagnostic devices. It is well recognized that dynamics of capillary filling of blood in a microfluidic channel may be non-trivially altered by mechanics over small scales.<sup>40</sup> In addition, many industrial applications over small scales find the use of shear-thickening fluids as well. The underlying transport characteristics may get even more involved considering the interplay of rheological interactions with the substrate wettability.<sup>31,41</sup> Recognizing such relevance, a few researchers have investigated the interfacial transport and contact line dynamics of non Newtonian fluids through narrow confinements, with one of the fluids being transported as non-

Newtonian.<sup>41–45</sup> However, no studies have yet been reported in the literature to capture the pertinent interactions with a driving electrical field in presence of electrokinetic effects.

Here, for the first time, we attempt to analyze the electric field driven contact line dynamics of a binary fluid system constituted by one non-Newtonian fluid, with particular emphasis on delineating a rich physical interplay of different forces arising due to rheological effects of the fluids and its coupling with the Maxwell stresses owing to electrokinetics and wetting phenomena over interfacial scales.<sup>31,41</sup> We bring out the consequent alterations on the capillary filling rate, which may have far ranging consequences in the design of various bio-microfluidic systems of practical relevance.

## II. Problem Formulation and Methodology

### A. Formulation of the problem and simulation set-up

We consider an external electric field driven transport of binary fluid system A/B, which contains one Newtonian and other non-Newtonian (power-law) fluid, through a narrow fluidic pathway. Figure 1 shows the set-up of our numerical simulations. In the numerical simulations, symmetric half of the channel is used owing to symmetric nature of the flow along the height of the channel. We consider the width of the channel to be much larger than its height, which, in effect, allows us to consider two-dimensional flow analysis. The height and length of the channel are  $2H$  and  $L$  respectively. The coordinate system is shown in Fig. 1, where the  $x$ -axis and  $y$ -axis are directed along the length and height of the channel respectively. We consider that the left side of the channel (i.e., up to a distance  $x = L_1$ ) is initially filled with fluid-A, whose density, viscosity and permittivity are  $\rho_A$ ,  $\mu_A$  and  $\varepsilon_A$  respectively. Fluid-B with density  $\rho_B$ , viscosity  $\mu_B$  and permittivity  $\varepsilon_B$ , on the other hand, initially residing at the right side and the remaining portion of the channel. We consider the walls of the channel to bear specified surface wettabilities as manifested in terms of static contact angle. We further consider both the walls of the channel to have a surface charge as manifested in terms of an equivalent zeta potential  $\zeta_0$ .

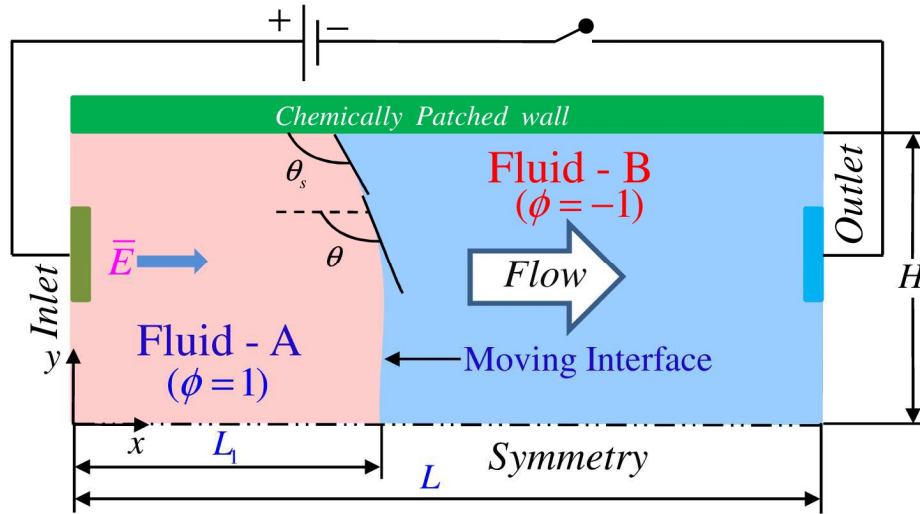


FIG. 1. (color online) Schematic describing the problem with physical dimensions. The solution domain is the symmetric upper-half of the channel and the origin is placed at the middle of the left end of the channel. Fluid A (light gray) resides in the left side of the channel and fluid B (deep gray) is at the right side of the channel. The wall is chemically patched. The applied electric field ( $\bar{E}$ ), actuates the flow. The angle  $\theta_s$  and  $\theta$  are the static contact angle at the wall and the slope of the interface respectively.

## B. Methodology

### 1. Phase field model

In the present study, we consider diffuse-interface based phase field model to describe the contact line motion of binary fluid systems. According to phase field method, the state of the binary fluid system at any spatiotemporal location is described by an order parameter  $\phi$ , which in the present case is characterized by the relative phase concentration of the respective phases,  $\phi = (n_1 - n_2)/(n_1 + n_2)$ , where  $n_1$  and  $n_2$  are the number density of molecules of Fluid-A and Fluid-B respectively. Therefore, in the present study,  $\phi = 1$  represents the displacing phase fluid (Fluid-A in the schematic) and  $\phi = -1$  represents the displaced phase fluid (Fluid-B in the schematic). The thermodynamic behavior of the binary fluid systems can be described by the Ginzburg-Landau free energy functional.<sup>46–53</sup>

$$F = \int_{\forall} \left\{ f(\phi) + \frac{1}{2} \sigma_{\xi}^2 |\nabla \phi|^2 \right\} d\forall \quad (1)$$

In Eq. (1),  $F$  is the total energy,  $\forall$  spans over the entire fluid domain. The coefficients  $\sigma$  and  $\xi$  can be linked to the interfacial tension and interface width respectively. The first term in Eq. (1) is the expression for the bulk free energy density of the binary fluid system, while the second term takes care of the interfacial free energy due to the presence of an interface separating the two fluids. We may cast the first term on the right hand side of Eq. (1) in the form of a double well potential which for an isothermal system can be written as:<sup>26,54,55</sup>

$$f(\phi) = \frac{\sigma}{\xi} (\phi^2 - 1)^2 \quad (2)$$

Two minima of the phase field variable  $\phi$  correspond to the two stable phases i.e., fluid-A and fluid-B respectively. The chemical potential ( $G$ ) is defined as the variational derivative of free energy functional with respect to the order parameter  $\phi$  and takes the following form:

$$G = \frac{\delta F}{\delta \phi} = f'(\phi) - \sigma \xi \nabla^2 \phi \quad (3)$$

## 2. Governing transport equations of the fluid motion

The governing transport equations for the problem considered in the present study are the continuity, momentum, Cahn-Hilliard equation for the interfacial movement, and the Poisson-Boltzmann equation for the charge distribution in the channel.

### 2.1 Cahn-Hilliard model for the interface movement

The convection-diffusion equation governing the evolution of the order parameter can be expressed in the form given below.<sup>12,13,46,49,52,56–59</sup>

$$\partial_t \phi + \mathbf{u} \cdot \nabla \phi = \nabla \cdot (M \nabla G) \quad (4)$$

In the above equation,  $\mathbf{u}$  is the velocity field,  $M$  is a constant that controls the diffusion across the interface and is termed as the mobility of the order parameter and  $G$  is the chemical potential as described by Eq. (3). The boundary conditions for Eq. (4) are given below:<sup>29</sup>

$$\mathbf{n} \cdot \nabla G = 0 \quad (5a)$$

$$\mathbf{n} \cdot \nabla \phi = -\tan\left(\frac{\pi}{2} - \theta_d\right) |\nabla \phi - (\mathbf{n} \cdot \nabla \phi) \mathbf{n}| \quad (5b)$$

In the above two equations,  $\mathbf{n}$  is the outward pointing normal coordinate. The first boundary condition as given in Eq. (5a) ensures no flux through the surface. In Eq. 5b,  $\theta_d$  is the dynamic contact angle, which is related to the static equilibrium contact angle by the Cox-Voinov relation as given by:<sup>60,61</sup>

$$\theta_d^3 = \theta_s^3 + 9 \text{Ca} \ln(R/l_{slip}) \quad (5c)$$

Here  $R$  is the macroscopic length scale,  $l_{slip}$  is the molecular slip length. In Eq. 5(c),  $\theta_s$  is the imposed static contact angle, the capillary number (Ca) is computed based on the local contact line velocity and the molecular slip-length is assumed to be of the order of the interface width.<sup>26</sup>

## 2.2 Charge Distribution: Poisson-Boltzmann equation and Laplace equation

An aqueous solution in contact with the solid surface develops an interfacial charge (independent of the application of any external electric field) that leads to the formation of thin region of net charge density close to the surface which is referred to as the Electric Double Layer (EDL).<sup>34</sup> The potential distribution in the EDL is described by the Poisson-Boltzmann equation.<sup>62</sup>

$$\nabla \cdot [\varepsilon \nabla \psi] = -\rho_e \quad (6)$$

In Eq. (6),  $\varepsilon$  is the permittivity of the fluid and  $\rho_e$  is the net electric charge density. The net electric charge density  $\rho_e$  can be described by the Boltzmann distribution, which for a  $z:z$  symmetric electrolyte takes the form as given below.<sup>34,63</sup>

$$\rho_e = -2\rho_0 \sinh(ze\psi/k_B T) \quad (7)$$

where  $\rho_0$  is the reference charge density,  $e$  is the protonic charge,  $k_B$  is the Boltzmann constant,  $z$  is the valance, and  $T$  is the absolute temperature. In Eq. (6), we use the following boundary conditions:

$$\psi(x, \pm H) = \zeta_0 \quad (8)$$

where  $\zeta_0$  is the potential (zeta potential) specified at the channel walls.

We further note that an externally applied axial voltage, which actuates the flow, also acts on the immiscible binary fluid system, in addition to the induced transverse field as mentioned above. The corresponding potential distribution ( $\psi^*$ ) will satisfy the following equation.<sup>38,63</sup>

$$\nabla \cdot [\varepsilon \nabla \psi^*] = 0 \quad (9)$$

The boundary conditions for Eq. (9) are given below:

$$\left. \begin{aligned} \psi^*(0, y) &= V_0 \\ \psi^*(L, y) &= 0 \\ \mathbf{n} \cdot \nabla \psi^*|_{y=\pm H} &= 0 \end{aligned} \right\} \quad (10)$$

### 2.3 Fluid flow equations

The diffusion of the order parameter across the interface contributes a body force term in the momentum equation, which couples the fluid flow description with that of the order parameter.<sup>13,48,49,52,64</sup> On the other hand, electrokinetic effects give rise to additional body force terms in the momentum equation.<sup>21,38</sup> Accordingly, one may write the continuity and the momentum conservation equations as:

$$\nabla \cdot \mathbf{u} = 0 \quad (11a)$$

$$\partial_t(\rho \mathbf{u}) + \nabla \cdot (\rho \mathbf{u} \otimes \mathbf{u}) = \nabla(-p\mathbf{I} + \tau) + G\nabla\phi + \rho_e \nabla \psi^* + (\mathbf{E} \cdot \mathbf{E}/2) \nabla \varepsilon + 1/2 \left( \nabla \left( \rho \partial_\rho \varepsilon (\mathbf{E} \cdot \mathbf{E}) \right) \right) \quad (11b)$$

The term  $\tau$  appearing in the first term in the right hand side of Eq. (11b) denotes the deviatoric stress, which may be modeled based on the constitutive behavior of the fluid under concern. In particular, for power law fluid,  $\tau = k\dot{\gamma}^n$ , where  $k$  is the flow consistency index,  $n$  is the flow behavior index ( $n < 1$  for shear thinning fluids, and  $n > 1$  for shear thickening fluids), and  $\dot{\gamma}$  is the rate of deformation. The second term in right hand side of Eq. (11b) arises because of the presence of an interface in the flow field, while the remaining three terms are the electrokinetic

body force terms. The penultimate term arises due to the spatial variation of permittivity and the last term is an outcome of electrostriction force that becomes significant when permittivity is a function of the density. We mention here that  $\mathbf{E}$  is the total electric field that accounts for both the EDL field ( $\psi$ ) and the applied electric field ( $\psi^*$ ).

To describe the fluid motion in the channel, no slip and no penetration boundary conditions ( $u = 0, v = 0$ ) are applied at the walls of the channel. Moreover, we assume that both the fluids are initially at rest. We further consider the inlet ( $p_{in}$ ) and outlet gauge pressures ( $p_{out}$ ) to be zero. In compliance with the phase field method, we consider that the permittivity, density and effective viscosity appearing in Eqs. (6), (9) and (11b) to be explicit functions of the order parameter and can be mathematically written as:<sup>12,36–38,41,49,52,53</sup>

$$\varepsilon = \varepsilon_A (1 + \phi) / 2 + \varepsilon_B (1 - \phi) / 2 \quad (12a)$$

$$\rho = \rho_A (1 + \phi) / 2 + \rho_B (1 - \phi) / 2 \quad (12b)$$

$$\mu_{eff} = \mu_{eff,A} (1 + \phi) / 2 + \mu_{eff,B} (1 - \phi) / 2 \quad (12c)$$

Note that  $\mu_{eff}$  in Eq. (12c) is the effective viscosity and can be expressed as:  $\mu_{eff} = k\dot{\gamma}^{n-1}$ . For the Newtonian fluid (i.e.,  $n = 1$ ),  $\mu_{eff}$  is the viscosity of the fluid. It is important to mention here that we have considered property matched binary fluids (permittivity, density and viscosity) in the present study and hence the last two terms of the momentum equation (Eq. 11b) drop out.

## 2.4 Non-dimensional equations

In order to cast the governing transport equations and the boundary conditions into non-dimensional form, we use following dimensionless variables:  $\bar{\psi}^* = \psi^* / (V_0 \xi / L)$ ;  $\bar{u}, \bar{v} = u, v / u_{ref}$ ;  $\bar{x}, \bar{y} = x, y / \xi$ ;  $\bar{\psi} = ze\psi / k_B T$ ;  $\bar{\mu}_{eff} = \mu_{eff} / \mu_{eff,ref}$ ;  $\bar{\rho} = \rho / \rho_{ref}$ ;  $\bar{\varepsilon} = \varepsilon / \varepsilon_{ref}$ ;  $\bar{p} = p / p_{ref}$  and  $\bar{t} = t / t_{ref}$ , where  $p_{ref} = \mu_{eff,ref} u_{ref} / \xi$ ;  $t_{ref} = \xi / u_{ref}$  and  $u_{ref} = \frac{\varepsilon_{ref} k_B T V_0}{ze \mu_{eff,ref} L}$ . The

chemical potential is non-dimensionalized as:  $\bar{G} = G / (\sigma / \xi)$ . With the aid of the dimensionless parameters mentioned above, finally, we arrive at the following set of dimensionless equations.

$$\text{Pe} \left[ \partial_t \phi + \mathbf{u} \cdot \bar{\nabla} \phi \right] = \bar{\nabla} \cdot (\bar{M} \bar{\nabla} \bar{G}) \quad (13)$$

$$\bar{\nabla} \left[ \varepsilon \bar{\nabla} \bar{\psi} \right] = \bar{\lambda}^2 \sinh(\bar{\psi}) \quad (14)$$

$$\bar{\nabla} \left[ \varepsilon \bar{\nabla} \bar{\psi}^* \right] = 0 \quad (15)$$

$$\bar{\nabla} \cdot \bar{\mathbf{u}} = 0 \quad (16)$$

$$\text{Re} \bar{\rho} \left[ \partial_t (\bar{\rho} \bar{\mathbf{u}}) + \bar{\nabla} \cdot (\bar{\rho} \bar{\mathbf{u}} \otimes \bar{\mathbf{u}}) \right] = \bar{\nabla} \cdot (-\bar{p} \mathbf{I} + \bar{\tau}) + \bar{\lambda}^2 \sinh(\bar{\psi}) \bar{\nabla} \bar{\psi}^* + (\bar{G}/\text{Ca}) \bar{\nabla} \phi \quad (17)$$

In the present study, we have considered the properties of power-law fluid to be the reference properties while non-dimensionalizing of the governing transport equations. The scheme of non-dimensionalisation gives rise to a few dimensionless parameters which are defined as: Peclet number,  $\text{Pe} = u_{ref} \xi^2 / M_c \sigma$ ; Capillary number,  $\text{Ca} = u_{ref} \mu_{eff,ref} / \sigma$  and Reynolds number,  $\text{Re} = \rho_{ref} u_{ref} \xi / \mu_{eff,ref}$ . We define  $\bar{M}$  as:  $\bar{M} = M / M_c$  where  $M_c$  is defined following reported MD simulation studies<sup>65</sup> as:  $M_c = C l^4 / \sqrt{m \varepsilon_e}$ ;  $l$  and  $\varepsilon_e$  being the length scale and energy scale respectively in the Lennard-Jones potential for fluid molecules and  $m$  being the molecular mass of fluid, and  $C$  is a constant ( $\approx 0.023$ ). The term  $\lambda$  in equation (14), which is called the inverse of Debye length, can be expressed as:  $\lambda = (2 \rho_{ref} z e / \varepsilon_{ref} k_b T)^{1/2}$  and  $\bar{\lambda} = \lambda \xi$ . In the present analysis,  $V_0/L \sim 10^4$  V/m, which makes,  $u_{ref} = 10^{-4}$  m/s.

### C. Numerical Method and Model Benchmarking

In the present study, we have used the finite element multiphysics framework of COMSOL<sup>®</sup> for solving the governing transport equations. We have used PARDISO solver and generalized- $\alpha$  scheme for temporal discretization. We have used uniform grid sizes of  $\Delta x, \Delta y = 0.2 \xi$  for all the simulations. It is important to mention in this context here that before applying the driving force to actuate bulk fluid motion, we initialize the phase field variable to

form the interface of co-existing two bulk phases ( $\phi = \pm 1$ ). Initialization of phase field variable, in essence, leads to an equilibrium interface profile following the solution of the equation:

$$G(\phi) = 0 \quad (18)$$

*Model Validation:* We have benchmarked the phase field model for the moving contact line problems using the results reported in Wang et al,<sup>46</sup> whose model and numerical framework are in turn benchmarked against molecular dynamic simulations.<sup>65</sup> In Fig. 2, we show the benchmarking results, where we show the variation of the contact line velocity for a pressure driven flow over a substrate having patterned wettability i.e., the substrate has periodic patches which preferentially like and dislike the incoming fluid stream. When the contact line moves over the chemically patterned surface, the moving interface has to dynamically adjust with the substrate affinity condition and has to switch between the interface profiles for the different patches. As the contact line moves from the favorable to the unfavorable stripe, the contact line undergoes an acceleration (de-pinning) and jumps to the favorable stripe where it tends to pin. This periodic pinning/depinning of the contact line, when it moves over the patterned substrate, is manifested as an oscillatory motion of the contact line as manifested in Fig. 2. We observe an extremely good agreement between the present and reported results<sup>46</sup>.

*Grid independence study* – The effects of grid size on the accuracy of the results have been shown in Fig. 2(b), which shows the variation of contact line velocity along the length of the channel for different grid sizes. One may clearly see from Fig. 2(b) that the variation becomes negligible as the grid size is reduced below  $\Delta x, \Delta y = 0.1\xi, 0.2\xi$ . Accordingly, the grid sizes  $\Delta x, \Delta y = 0.2\xi$  have been considered for all our subsequent studies.

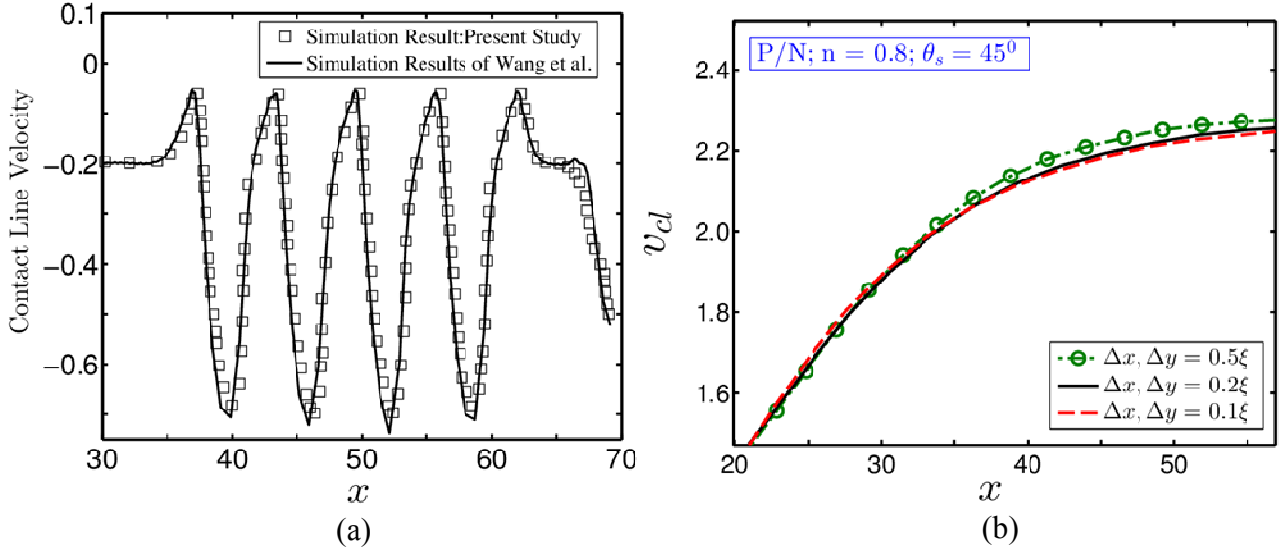


FIG. 2. (a) **Model benchmarking.** Contact line velocity shown as a function of distance along the capillary. The simulation results using the present model are represented by the solid lines and the square markers are used to represent the results reported by Wang et al.<sup>46</sup>. The results of the present numerical simulations and the reported numerical experimental results are in perfect match. b) **Grid independence study:** Contact line velocity as a function of the location along the channel for three different values of grid sizes.

We further mention that from here onwards the overbars used to represent non-dimensional quantities will be dropped from the variable nomenclature for the ease of representation.

### III. RESULTS AND DISCUSSIONS

Here, we present the rheology-modulated contact line motion of the binary fluid system and show the intriguing interfacial dynamics owing to competing effects of the fluid rheology and its interaction with the electrical forcing and surface wettability. We consider different flow configurations like Newtonian fluid displacing power-law fluid (N/P) and vice versa (P/N). It is important to mention here that we use the following dimensionless parameters in the present study unless otherwise specified:  $Re = 0.01$ ,  $Pe = 0.02$ ,  $Ca = 0.1$ ,  $\zeta_0 = -4$ ,  $\lambda = 0.2$ . These values are in accordance with the typical parameters encountered in microfluidic setups<sup>21,25,41,46,49</sup>. It is important to mention here that while discussing the results, we will refer to the static contact angle values ( $\theta_s$ ) as reference parameters, even though the model takes into

account the dynamic contact angles ( $\theta_d$ ), which are computed dynamically depending on the local contact line velocity as the interface evolves.

### A. Contact Line velocity

We start our discussion with Figs. 3(a) - (c), which show the variation of contact line velocity ( $v_{cl}$ ) of a two fluid system as considered in the present study. While investigating the contact line velocity, we consider three different values of static contact angle  $\theta_s = 45^\circ, 90^\circ$  and  $135^\circ$  in the analysis.

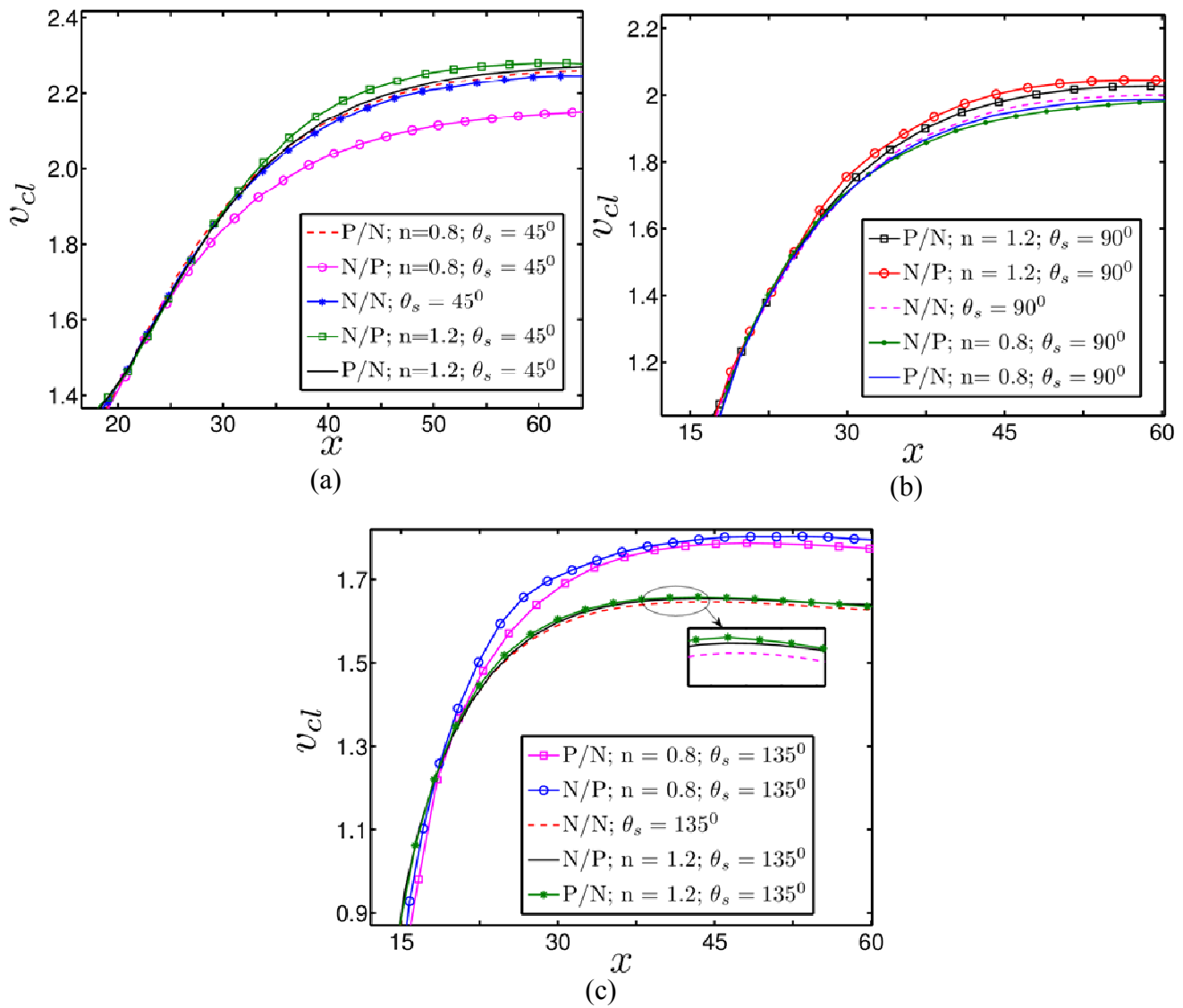


FIG. 3. (Color online) Variation of contact line velocity ( $v_{cl}$ ) vs. distance along the channel ( $x$ ) for different flow configurations obtained at three different surface wetting conditions of the wall: (a)  $\theta_s = 45^\circ$ , (b)  $\theta_s = 90^\circ$  and (c)  $\theta_s = 135^\circ$ . P/N refers to power-law fluids (both shear-thickening and shear-thinning) displacing Newtonian fluid, while N/P indicates the reverse situation. N/N refers to Newtonian fluid is displacing another Newtonian fluid. For  $\theta_s = 45^\circ$ , appreciable difference in contact line velocity is seen for the cases when receding fluids are power-law fluids. On the other hand, for the cases with advancing fluids as power-law fluids, the variation of contact line velocity does not show any significant difference with the alterations in the value of  $n$ . The contact line velocity for  $\theta_s = 135^\circ$  becomes higher when receding fluid is shear-thinning and lower when it is a shear-thickening fluid.

The contact line velocity ( $v_{cl}$ ) initially shows an increasing trend for all the cases considered. The initial increasing trend of  $v_{cl}$  can be attributed to the sudden driving force experienced by the binary fluid system owing to the application of an external electric field, which compels the interface to accelerate along the capillary. Moreover, as the interface starts moving along the channel, it has to dynamically adjust to the contact angle specified at the solid substrate. However, the contact line velocity further downstream of the channel attains a steady profile for all the cases considered, as can be seen from Figs. 3(a)-(c).

Once the contact line velocity reaches its steady value, significant differences in the velocity profile are observed with the alterations in  $\theta_s$  and  $n$ . One can observe from Figs. 3(a)-(b) that the contact line velocity for the cases of  $\theta_s = 45^\circ$  and  $90^\circ$  becomes maximum and minimum when a Newtonian fluid displaces the shear-thickening (N/P curve;  $n = 1.2$ ) and shear-thinning (N/P curve;  $n = 0.8$ ) fluids respectively. On the other hand, a reverse scenario is observed in Fig. 3(c) for the variation of contact line velocity for  $\theta_s = 135^\circ$ . In an effort to explain this, we would like to mention here that the advancement of the interface at the three phase contact line essentially depends upon the competition of three important forces: the surface tension force, the electrical forcing, and the viscous drag. The marked difference in contact line velocity can be correlated to the presence of different topographical features of the two-fluid system under different conditions, as modulated by these forces. Different topographical features, in turn, will alter the viscous drag and its interplay with the surface tension forces as well as the

Maxwell stresses. The alteration in the net force will, in turn, result in an observable difference in contact line velocity as reflected in Figs. 3(a)-(c).

In an effort to bring out the quantitative assessment about the variation of different forces across the contact line for the different cases, in Fig. 4, we show the variation of net force acting across the contact line  $F_{x|cl}$  as the interface moves along the channel. In Figs. 4(a), we show the variation of the net force by swapping the rheology of the driving and the driven fluids by keeping the flow behavior index ( $n$ ) and electrical forcing unaltered for  $\theta_s = 45^\circ$ . For the case when shear-thinning fluid is the advancing one (P/N curve;  $n = 0.8$ ), the net driving force acting across the contact line increases as attributable to a reduced magnitude of the viscous drag. Fig. 4(b) shows the variation of net force with variation in the flow behavior index ( $n$ ) of the receding fluid; advancing fluid being the Newtonian one in both the cases. It is clearly evident that the net force increases with increase in  $n$ . This is primarily due to the reduction in the magnitude of the viscous drag with increases in  $n$ . We further show, in Fig. 4(c), that for the case when receding fluid is shear-thinning (N/P curve,  $n=0.8$ ), the net force acting over the contact line becomes lower for  $\theta_s = 135^\circ$ , which again underlines the favorable effect of surface tension force intrinsically attached with  $\theta_s = 45^\circ$ . It is important to mention in this context here that the variation of net force acting across the contact line as delineated above are in clear support of the variation of contact line velocities as observed in Figs. 3(a)-(c).

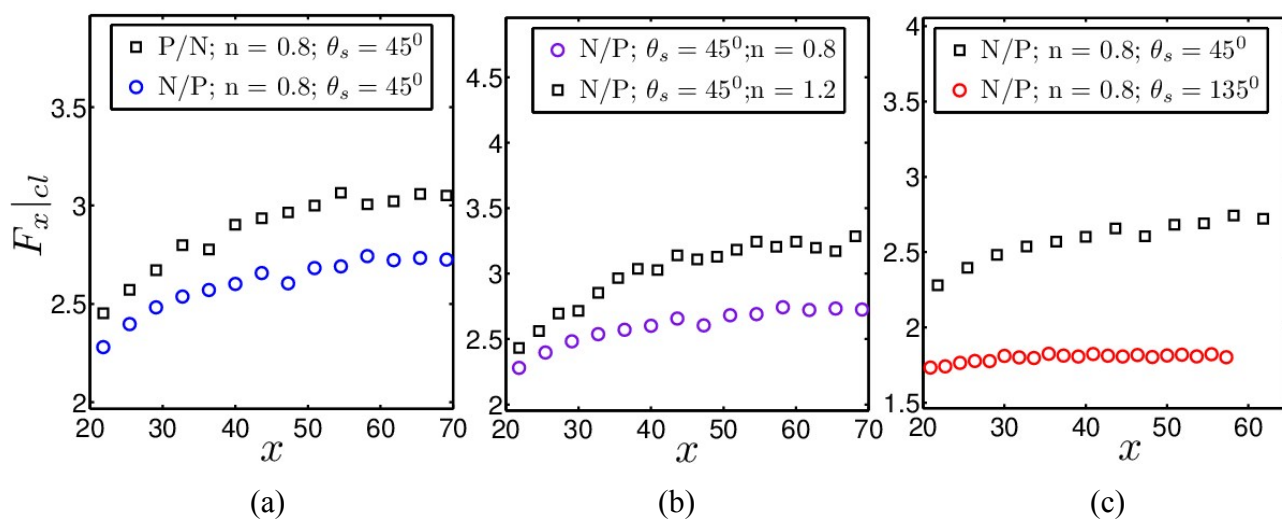


FIG. 4. (Color online) Variation of net force acting across the contact line for different cases.

## B. Interface Bending

The flow displacement in the capillary is largely manifested by the interfacial shape of the immiscible binary fluid system. We show, in Fig. 5, the shapes of the interface obtained for different cases. It is important to mention in this context here that all the interface contours as shown in Fig. 5 correspond to flow time  $t = 15$ . Figure 5 suggests that for all the cases of static contact angles considered, when Newtonian fluid is displacing the shear-thickening fluid in the capillary (N/P curve;  $n = 1.2$ ), the interface shows more bending towards the receding fluid. On the other hand, for the same flow configuration, when the receding fluid is shear-thinning (N/P curve;  $n = 0.8$ ), the interface meekly bends toward the receding fluid. It is noteworthy to observe from Fig. 5 that for the cases when advancing fluid is non-Newtonian (both shear-thinning and shear-thickening), the interface deviates mildly with the alterations in the substrate wettability. The electrical forcing acting over the interface within the EDL makes an effort to drag the interface along the capillary, while the interplay between surface tension force and viscous drag creates either a reverse or favorable impact on the interface movement depending upon the flow configurations and substrate wettability.

In an effort to analyze the effect of fluid rheology on the interface shape, we show, in Fig. 6, the variation of velocity gradient normal to the channel wall  $u_n (= \partial u / \partial n)$  at time  $t = 15$  for different cases. Note that the interface assumes a steady profile at  $t = 15$ . We can argue from Figs. 6(a)-(b) that, for both the cases of  $\theta_s$  ( $= 45^\circ$  and  $135^\circ$ ) and specific to the case of flow configuration where the receding fluid is shear-thinning (N/P curve;  $n = 0.8$ ), the magnitude of normal velocity gradient at the three phase contact line is more. Since, we have used phase field method in the present study; the model automatically introduces a slip at the three phase (fluid-fluid-solid) contact line. For a given slip length provided by the model itself, the higher velocity gradient at the contact line for the case when the receding fluid is shear-thinning (N/P curve;  $n = 0.8$ ) produces more slip velocity for both the cases of surface wettability considered. Relatively larger slip velocity corresponding to this kind of flow configurations (Newtonian fluid

displacing shear-thinning fluid) allows the contact line to move forward, and in effect, reduces the interface bending as can be seen in Figs. 5(a) and (c).

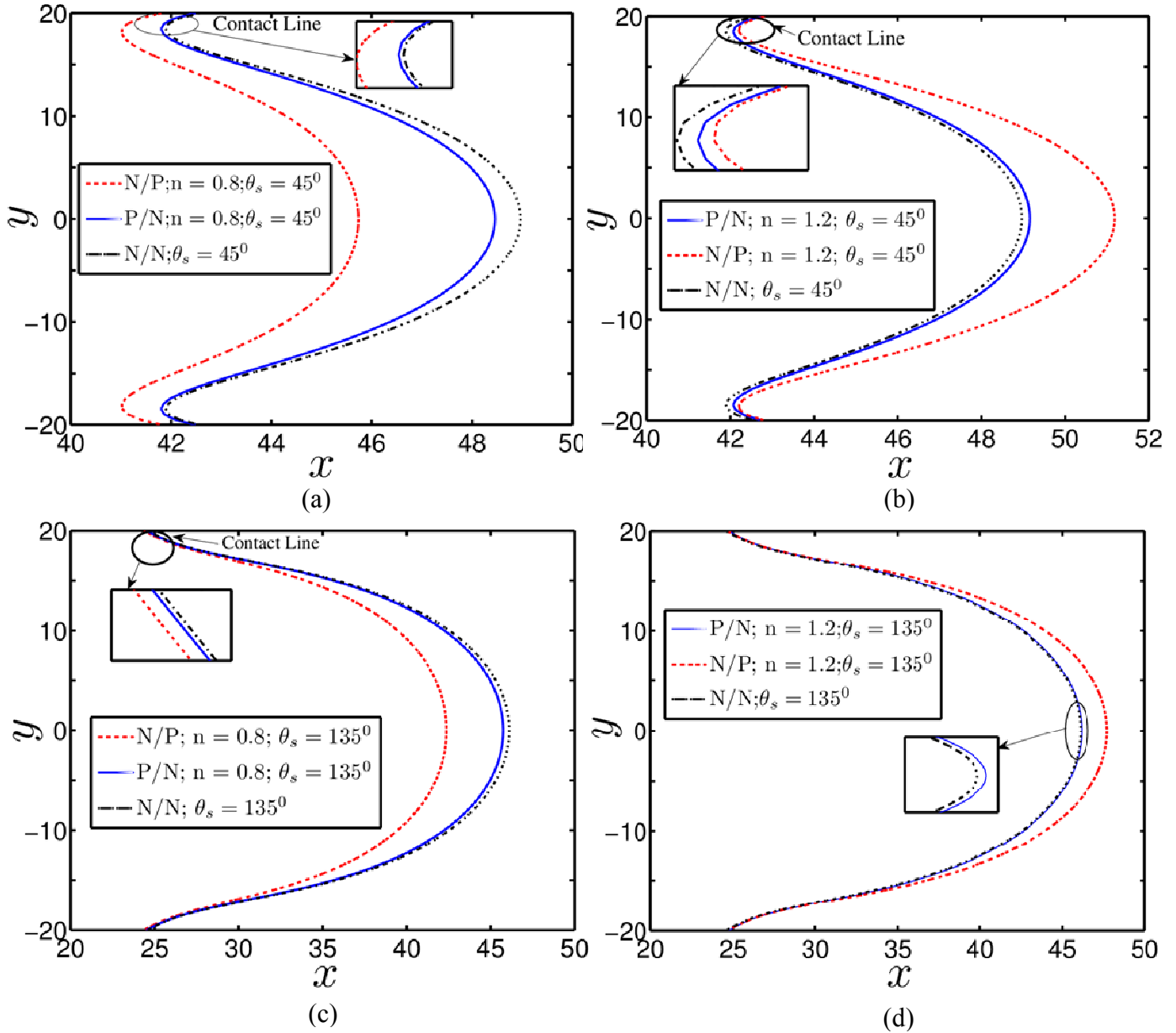


FIG. 5. (Color online) Interface evolution in the flow as shown by its shape for different cases at a given time  $t = 15$ . The shape of interface shows insignificant difference with the alterations in surface wettability for the cases when advancing fluids are non-Newtonian (both shear-thinning and shear-thickening).

However, a precise look at Figs. 5(a) and (c) clearly unveils that the interface mildly bends towards the receding fluid for the case of  $\theta_s = 45^\circ$ , while the interface severely bends in the direction of receding fluid for  $\theta_s = 135^\circ$ , which essentially underlines the influence of surface tension force on the interface bending phenomena. We also note from the present figures that the location of contact line may change appreciably with the alteration in flow configuration (see inset of Fig. 5) while keeping the other relevant parameters unaltered. On the contrary, when the receding fluid is shear-thickening ( $n = 1.2$ ), the velocity gradient at the three phase contact line for all the cases of  $\theta_s$  is relatively less (see Figs. 6a,b). The relatively lesser magnitude of normal velocity gradient produces small amount of slip velocity at the contact line. The small slip velocity for this particular flow configuration makes an obligatory situation for the interface to show a tendency of pinning at the contact line, which eventually results in a higher bending as one can foresee from Figs. 5(b) and (d). We further confirm from Fig. 7 that for a given surface wettability, the magnitude of velocity gradient normal to the wall ( $u_n$ ) remains almost invariant for the case when advancing fluid is non-Newtonian (both the shear-thickening and shear-thinning).

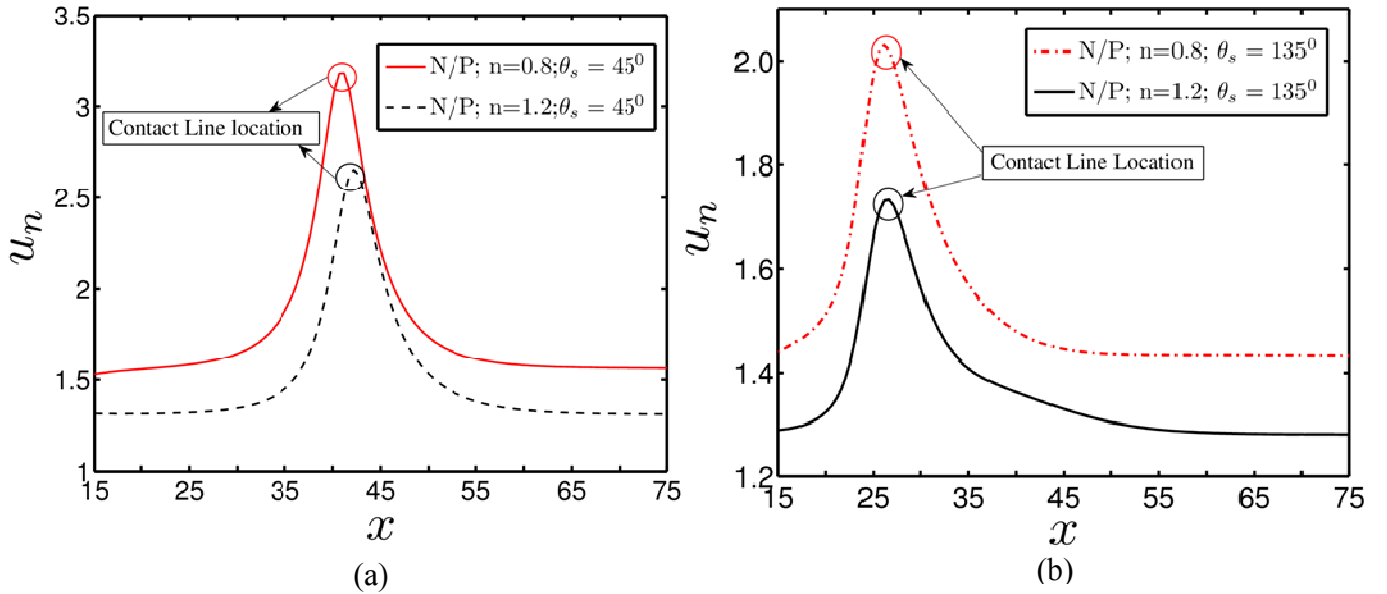


FIG. 6. (Color online) Velocity gradient normal to the channel wall for the case when advancing fluid is Newtonian for two different surface wetting conditions:  $\theta_s = 45^\circ$  and  $135^\circ$  respectively. The velocity gradient shown above corresponding to flow time  $t = 15$ . For a given static contact angle ( $\theta_s$ ), a

significant difference in normal velocity gradient ( $u_n$ ) is observed for all the case when receding fluid is shear-thinning fluid (N/P curve;  $n = 0.8$ ).

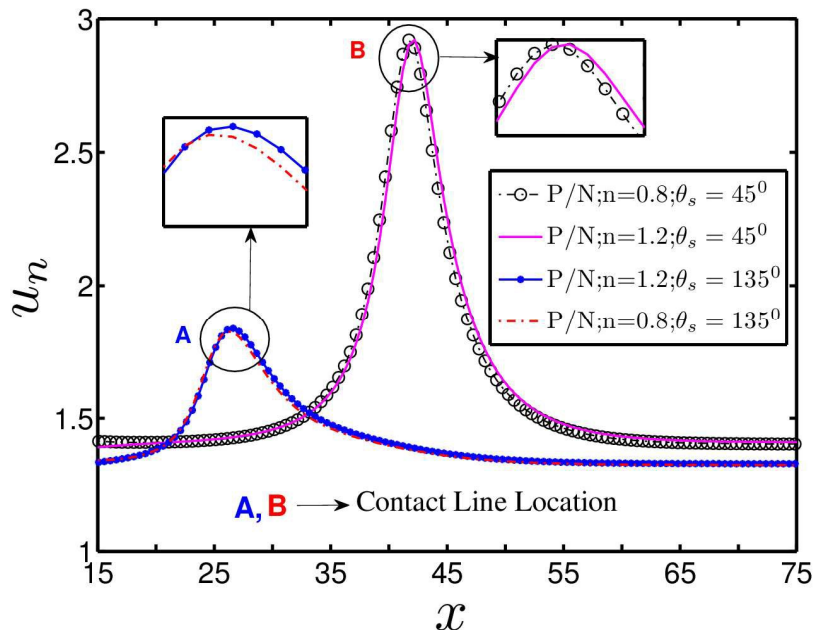


FIG. 7. (Color online) Velocity gradient normal to channel wall for the cases when advancing fluids are shear-thickening and shear-thinning for two different static contact angles:  $\theta_s = 45^\circ$  and  $135^\circ$  respectively. The velocity gradient shown above corresponding to  $t = 15$ . For a given  $\theta_s$ , no significant difference in the normal velocity gradient ( $u_n$ ) is observed with the alterations in the rheological combinations.

In order to obtain deeper insights on the interface bending phenomenon, in Figs. 8(a)-(b), we show the slope of the interface vs.  $y$  for different flow configurations. Note that all the curves depicting the slope of the interface are obtained at  $t = 15$ . A closer scrutiny of Fig. 8 clearly reveals that the slope of the interface increases within the EDL, which is as expected. One can anticipate from Figs. 8(a) & (b) that, for both the cases of  $\theta_s$  ( $90^\circ$  and  $135^\circ$ ), the curvature of the interface is more when shear-thickening fluid (N/P curve;  $n = 1.2$ ) is the receding fluid, whereas the interface curvature is less when receding fluid is shear-thinning (N/P curve;  $n = 0.8$ ). The above discussion implicates that the interface will bend strongly towards the displaced phase fluid when Newtonian fluid is displacing the shear-thickening fluid, disregarding the effects of surface wettability and this observation is nicely confirmed on the variation of interface shape as depicted in Fig. 5.

We would like to discuss an important point here that, during the evolution of the interface, the contact angle usually shows an hysteretic behavior, which primarily arises due to the mismatch between the advancing contact angle in dynamic condition and the static contact angle imposed over the surface. However, we do not observe any such hysteretic behavior of the contact line in the present study as envisaged from Figs. 8(a)-(b). The physical explanations behind the absence of contact angle hysteresis are as follows: The boundary condition, which takes the effect of surface wettability into the model used in the present study, allows the interface profile to follow the contact angle specified even during dynamic condition and hence, does not tolerate the hysteretic behavior.

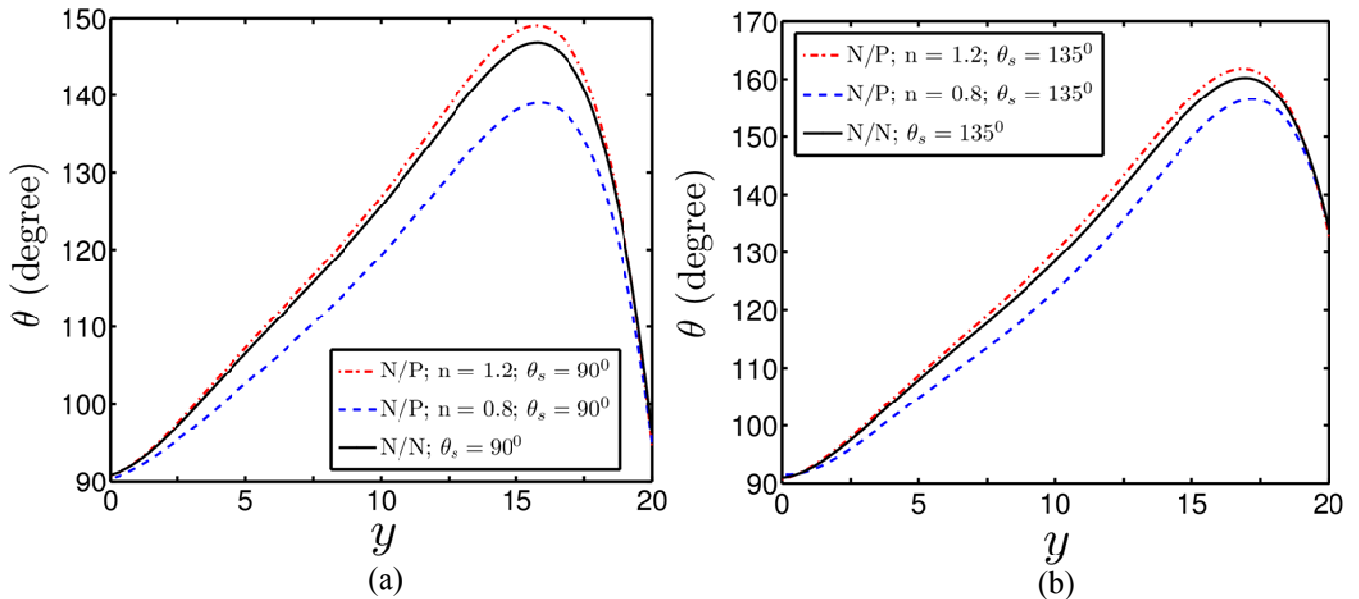


FIG. 8. (Color online) Interface slope for the cases when advancing fluid is Newtonian and receding fluids are non-Newtonian (both shear-thinning and shear-thickening) obtained at flow time  $t = 15$  for different surface wetting conditions: (a)  $\theta_s = 90^\circ$  and (b)  $\theta_s = 135^\circ$ . The angle  $\theta$  represents the angle made by the line tangent to the interface with the solid substrate as shown in Fig. 1. The curvature of the interface is more when shear-thickening fluid ( $n = 1.2$ ) is the receding fluid, and less when receding fluid is shear-thinning ( $n = 0.8$ ).

We have, so far, shown that the alteration in flow configurations clearly alter the contact line motion over interfacial scales due to drastic change in the viscous drag as modulated by the electrical forcing and surface wettability. We have quantified the net force acting across the contact line due to intricate interplay of different forces as well. In order to bring out the unique effect of electrical forcing on the rheology driven interfacial dynamics, we next attempt to

compare the variation of the contact line velocity and the evolution of the interface in the capillary considering an applied pressure gradient that gives rise to the same average velocity as that of the driving electric field considered here, while keeping the flow configuration and other common parameters unaltered. In doing so, we probe into the variation of the contact line velocity and interfacial dynamics considering  $\theta_s = 135^\circ$ , when the receding fluids are shear-thinning ( $N/P; n = 0.8$ ) and shear-thickening ( $N/P; n = 1.2$ ) respectively.

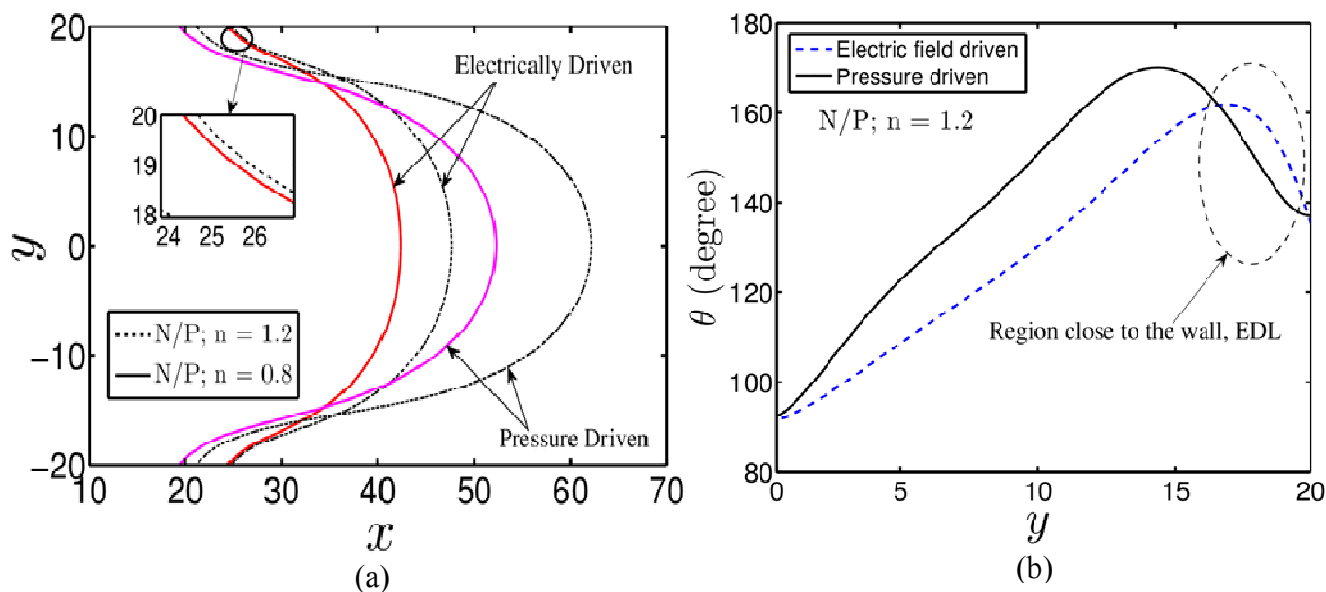


FIG. 9. (Color online) (a) Time sequence plot of interface position for the cases when receding fluids are non-Newtonian ( $N/P; n = 0.8$  and  $1.2$ ) corresponding to flow time  $t = 15$ , (b) Slope of the interface of binary fluids for a case when receding fluid is shear-thickening ( $N/P; n = 1.2$ ). Both the figures correspond to  $\theta_s = 135^\circ$ . Slope of the interface in the electric field driven flows is higher in the region very close to the wall (i.e., within EDL) as compared to pressure driven flows albeit all other conditions remain unchanged. Interface in electrically driven flows mildly bends toward the receding fluid.

Figure 9 shows the variation of interface shape and slope of the interface for both electrically and pressure driven flow environments. In plotting Fig. 9, we consider that non-Newtonian fluids (both shear-thinning and shear-thickening) are getting displaced by the Newtonian fluid ( $N/P; n = 0.8$  and  $1.2$ ) for the case of  $\theta_s = 135^\circ$ . It is important to mention here that all the interface contours shown in Fig. 9(a) correspond to flow time  $t = 15$ . Note that, for a given set of simulation parameters *viz.*, the property ratios and the static contact angle, the

interface in a pressure driven flow severely bends toward the receding fluid as compared to that of the electrically driven flows, which is primarily attributed to the nature of forcing acting over the interface.

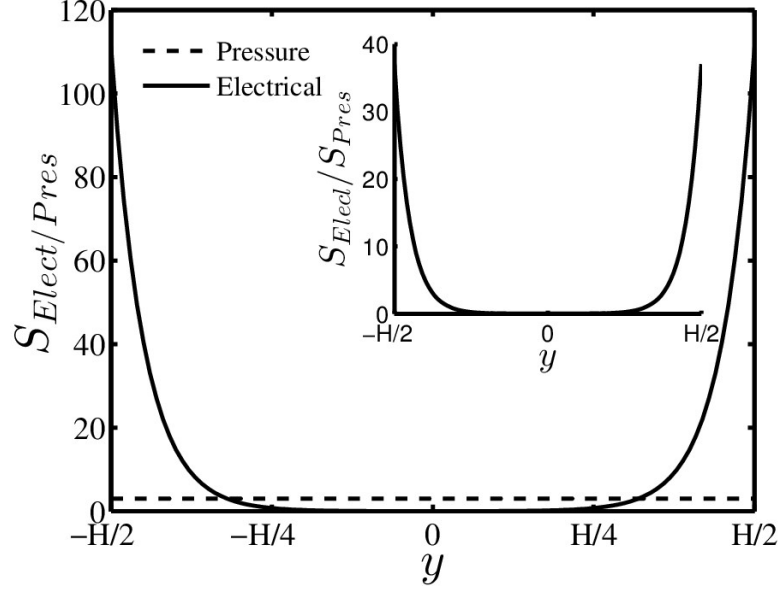


Fig. 10. Variation of the forces acting along the direction transverse to the channel.

In order to understand the distinctive natures of forcing in the two cases, we compute the forces driving transport in the two cases. The surface tension force behaves similarly in both the cases. The body force due to pressure gradient, driving unit average velocity through the channel is  $S_{\text{Pres}}|_{u_{av}=1} = 12\mu_{\text{eff}}/H^2$ . Using Debye-Huckel linearization, the electrical body force, which leads

to unit average velocity takes the form  $S_{\text{Elect}}|_{u_{av}=1} = \frac{(\mu_{\text{eff}}/\lambda)^2 \cosh(y/\lambda)}{\cosh(H/(2\lambda))} \left[ 1 - \frac{\tanh(H/(2\lambda))}{H/(2\lambda)} \right]^{-1}$ . In

Fig. 10, we show the variation of the two body forces ( $S_{\text{Elect}}, S_{\text{Pres}}$ ) along the direction transverse to the channel. It is important to note that in electrically driven flows, the driving force is mainly confined over a small region very close to the wall, i.e., inside the EDL (which scales with  $\lambda$ ) which is in sharp contrast to the pressure driven flow configuration where the driving force is acting over the complete lateral extent. As a result, the contact line moves at a faster pace in electrically driven flow as compared to the pressure driven configuration. On the other hand, in the pressure driven configuration, the interface along the centerline of the channel moves at a

faster rate as compared to the electrically actuated capillary transport, for the same average flow velocity. These two features can be seen clearly from the interface profiles shown in Fig. 9(a). As a result of the abovementioned effects, the point of inflection appearing in the interface profile is pushed towards the EDL in electrically actuated transport configuration which is clear from Fig. 9(b), where we show the slope of the interface separating the binary fluids. From Fig. 9(b) it is easily perceptible that the deformation of the interface within the EDL is large as compared to the pressure driven transport scenario.

### C. Filling Dynamics: Length of the advancing fluid

We have highlighted the rheological effects of the fluid as modulated by the electrical forcing and the wetting characteristics of the solid substrate on the interface bending phenomena in the preceding section. The primary objective of obtaining the interfacial shape of the binary fluid system was to predict the flow displacement in the capillary, which, in turn, dictates the length of the advancing liquid column in the capillary. Here we focus on the effects of the fluid rheology and surface wettability on the filling dynamics. In particular, we show, in Fig. 11, the variation of the length of the advancing liquid column in the capillary for different flow configurations. It is noteworthy to observe from Fig. 11 that, for both the values  $\theta_s$  considered in the present analysis, the time taken by the advancing fluid (Newtonian) to fill a certain length of the capillary increases when receding fluid is shear-thinning (N/P curve;  $n = 0.8$ ), while for the cases when shear-thickening fluid is the receding fluid (N/P curve;  $n = 1.2$ ), the required time decreases. Moreover, one can see that for the range of surface wettabilities considered, the filling time for the cases when advancing fluids are non-Newtonian (either shear-thinning or shear-thickening fluid) are comparable with the cases when both the receding and advancing fluids are Newtonian.

Figures 4 and 5 indicate that the alteration in fluid rheology and its interaction with the electrokinetic effect strongly affects the interface bending phenomena of two-fluid system following the net force acting across the contact line. Therefore, it is quite reasonable to expect that the time required by the advancing fluid to move a certain length along the capillary will indeed depend on the evolution of the interface of two-fluid system, which will, in turn, severely

depend on the particular combinations on hand, as confirmed in Fig. 11. Notably, the negligible differences in the variation of interfacial shape for the cases when both the non-Newtonian (shear-thinning and shear-thickening) as well as Newtonian fluids displacing another Newtonian fluid (P/N and N/N curve) as seen in Fig. 5 are in clear support of the filling times depicted in Fig. 11.

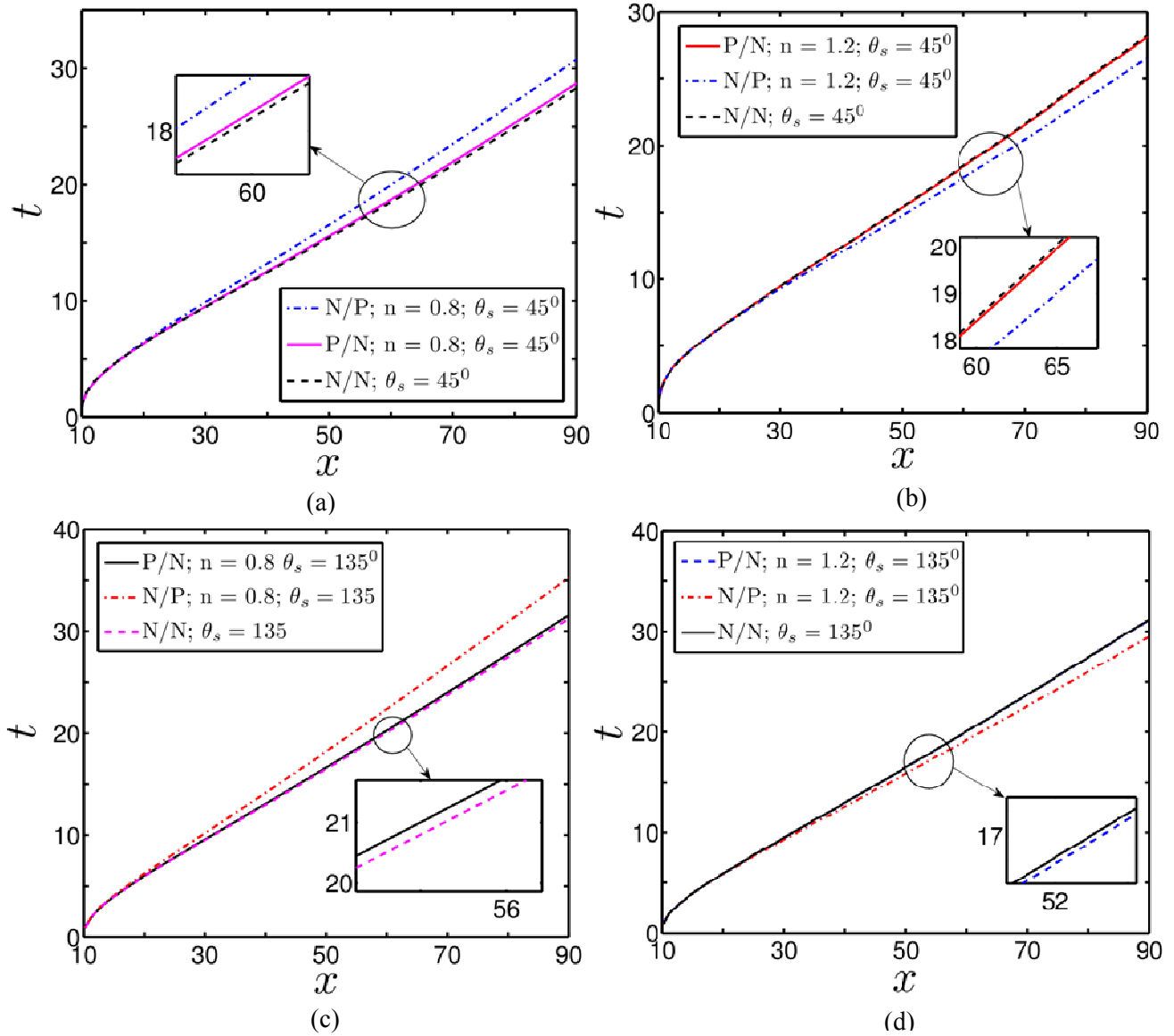


FIG. 11. (Color online) Variation of the length of the advancing liquid column in the capillary for different cases. For both the cases of surface wettability, the time ( $t$ ) taken by the advancing fluid to reach a certain length of the capillary becomes more when advancing and receding fluids are

Newtonian and shear-thinning ( $n = 0.8$ ) respectively, while the same decreases when advancing and receding fluids are shear-thickening ( $n = 1.2$ ) and Newtonian respectively.

#### IV. CONCLUSIONS

In the present study, we have investigated the rheology modulated contact line dynamics of a binary fluid system acted upon by an externally applied electric field in presence of EDL phenomena. The study reveals that the rheological effects of the fluids, in conjunction with electrical forcing and substrate wettability, play a crucial role on the interfacial electro-chemical-hydrodynamics, which, in turn, alters the interface shape and the length of the advancing liquid column into the capillary. For  $\theta_s = 45^\circ$ , perceptible difference in the contact line velocity is seen with the alterations in the flow behavior index for the cases when receding fluids are power-law fluids. On the other hand, for the cases with advancing fluids as power-law fluids, the variations in the contact line velocity are not significant with the alterations in the flow behavior index. Furthermore, the contact line velocity for  $\theta_s = 135^\circ$  becomes higher when receding fluid is shear-thinning and lower when it is a shear-thickening fluid, primarily attributable to the intricate variations in the viscous drag acting over the three-phase contact line. Thus, it can be inferred that the combination of rheology and wettability can be judiciously used for controlling electrokinetically driven contact line motion of binary fluid systems. We believe that the present study may enhance the understanding of filling dynamics from a fundamental perspective of contact line motion which may bear far reaching consequences in potential application in lab-on-a-chip based microfluidic devices, which are commonly used for the transportation of non-Newtonian biofluids such as blood.

#### ACKNOWLEDGEMENTS

PKM and SC gratefully acknowledge the Sponsored Research Industrial Consultancy (SRIC), Indian Institute of Technology Kharagpur, for providing the financial support under the Project, "Center of Excellence for Research and Training in Microfluidics (CEM)" for this research.

#### REFERENCES

1. Y. D. Shikhmurzaev, *Int. J. Multiph. Flow*, 1993, **19**, 589–610.

2. W. Boender, A. K. Chesters and A. J. J. van der Zanden, *Int. J. Multiph. Flow*, 1991, **17**, 661–676.
3. A. J. J. Van der Zanden and A. K. Chesters, *Int. J. Multiph. Flow*, 1994, **20**, 789–798.
4. A. J. J. van der Zanden and A. K. Chesters, *Int. J. Multiph. Flow*, 1994, **20**, 775–787.
5. F. Mugele, *Soft Matter*, 2009, **5**, 3377.
6. C. Bakli and S. Chakraborty, *Soft Matter*, 2015, **11**, 161–168.
7. L. Fraštia, A. J. Archer and U. Thiele, *Soft Matter*, 2012, **8**, 11363.
8. T. Kajiyama, A. Daerr, T. Narita, L. Royon, F. Lequeux and L. Limat, *Soft Matter*, 2013, **9**, 454.
9. G. Miquelard-Garnier, A. B. Croll, C. S. Davis and A. J. Crosby, *Soft Matter*, 2010, **6**, 5789.
10. R. Dey, K. Raj M, N. Bhandaru, R. Mukherjee and S. Chakraborty, *Soft Matter*, 2014, **10**, 3451–62.
11. O. V. Voinov, *Int. J. Multiph. Flow*, 1996, **22**, 1155–1166.
12. M. Ahmadlouydarab, Z.-S. (Simon) Liu and J. J. Feng, *Int. J. Multiph. Flow*, 2011, **37**, 1266–1276.
13. H. A. Akhlaghi Amiri and A. A. Hamouda, *Int. J. Multiph. Flow*, 2014, **61**, 14–27.
14. M. J. A. Hore and M. Laradji, *J. Chem. Phys.*, 2010, **132**, 024908.
15. L. M. Pismen, *Phys. Fluids*, 1982, **25**, 3.
16. W. Ren, *Phys. Fluids*, 2011, **23**, 072103.
17. D. N. Sibley, A. Nold, N. Savva and S. Kalliadasis, *Phys. Fluids*, 2013, **25**, 092111.
18. C. Bakli and S. Chakraborty, *J. Chem. Phys.*, 2013, **138**, 054504.
19. S. De Luca, B. D. Todd, J. S. Hansen and P. J. Daivis, *J. Chem. Phys.*, 2013, **138**, 154712.
20. M. Campisi, D. Accoto and P. Dario, *J. Chem. Phys.*, 2005, **123**, 204724.
21. P. K. Mondal, U. Ghosh, A. Bandopadhyay, D. DasGupta and S. Chakraborty, *Soft Matter*, 2014.

22. C. L. Moraila-Martínez, M. A. Cabrerizo-Vílchez and M. A. Rodríguez-Valverde, *Soft Matter*, 2013, **9**, 1664.
23. F.-C. Wang and H.-A. Wu, *Soft Matter*, 2013, **9**, 5703.
24. A. Askounis, D. Orejon, V. Koutsos, K. Sefiane and M. E. R. Shanahan, *Soft Matter*, 2011, **7**, 4152.
25. X. Luo, X.-P. Wang, T. Qian and P. Sheng, *Solid State Commun.*, 2006, **139**, 623–629.
26. D. Jacqmin, *J. Fluid Mech.*, 2000, **402**, 57–88.
27. P. Seppecher, *Int. J. Eng. Sci.*, 1996, **34**, 977–992.
28. A. Briant and J. Yeomans, *Phys. Rev. E*, 2004, **69**, 031603.
29. H. Ding and P. Spelt, *Phys. Rev. E*, 2007, **75**, 46708.
30. D. DasGupta, P. K. Mondal and S. Chakraborty, *Phys. Rev. E*, 2014, **90**, 023011.
31. S. Chakraborty, *Anal. Chim. Acta*, 2007, **605**, 175–84.
32. B. Ray, P. D. S. Reddy, D. Bandyopadhyay, S. W. Joo, A. Sharma, S. Qian and G. Biswas, *Electrophoresis*, 2011, **32**, 3257–67.
33. A. Bandopadhyay, D. DasGupta, S. K. Mitra and S. Chakraborty, *Phys. Rev. E*, 2013, **87**, 033006.
34. J. H. Masliyah and S. Bhattacharjee, *Electrokinetic and Colloid Transport Phenomena*, Wiley, 2006.
35. S. Das and S. Chakraborty, *Anal. Chim. Acta*, 2006, **559**, 15–24.
36. Y. Lin, P. Skjetne and A. Carlson, *Int. J. Multiph. Flow*, 2012, **45**, 1–11.
37. Q. Yang, B. Q. Li and Y. Ding, *Int. J. Multiph. Flow*, 2013, **57**, 1–9.
38. P. K. Mondal, U. Ghosh, A. Bandopadhyay, D. DasGupta and S. Chakraborty, *Phys. Rev. E*, 2013, **88**, 023022.
39. C. Bakli and S. Chakraborty, *Appl. Phys. Lett.*, 2012, **101**.
40. S. Chakraborty, *Lab Chip*, 2005, **5**, 421–430.
41. P. Yue and J. J. Feng, *J. Nonnewton. Fluid Mech.*, 2012, **189-190**, 8–13.

42. P. Yue, C. Zhou, J. J. Feng, C. F. Ollivier-Gooch and H. H. Hu, *J. Comput. Phys.*, 2006, **219**, 47–67.
43. P. Yue, J. J. Feng, C. Liu and J. Shen, *J. Nonnewton. Fluid Mech.*, 2005, **129**, 163–176.
44. D. E. Weidner and L. W. Schwartz, *Phys. Fluids*, 1994, **6**, 3535.
45. Y. Wang and K.-Q. Zhu, *Phys. Fluids*, 2014, **26**, 052103.
46. X.-P. Wang, T. Qian and P. Sheng, *J. Fluid Mech.*, 2008, **605**, 59.
47. D. M. Anderson, G. B. McFadden and A. A. Wheeler, *Annu. Rev. Fluid Mech.*, 1998, **30**, 139–165.
48. D. Jacqmin, *J. Comput. Phys.*, 1999, **155**, 96–127.
49. V. E. Badalassi, H. D. Ceniceros and S. Banerjee, *J. Comput. Phys.*, 2003, **190**, 371–397.
50. Z. Xu and P. Meakin, *J. Chem. Phys.*, 2009, **130**, 234103.
51. D. Borzacchiello, E. Leriche, B. Blottière and J. Guillet, *J. Nonnewton. Fluid Mech.*, 2013, **200**, 52–64.
52. Y. Q. Zu and S. He, *Phys. Rev. E*, 2013, **87**, 043301.
53. H. Liu, A. J. Valocchi, Y. Zhang and Q. Kang, *Phys. Rev. E*, 2013, **87**, 013010.
54. L. Pismen and Y. Pomeau, *Phys. Rev. E*, 2000, **62**, 2480–2492.
55. Y. Y. Yan and Y. Q. Zu, *J. Comput. Phys.*, 2007, **227**, 763–775.
56. J. W. Cahn and J. E. Hilliard, *J. Chem. Phys.*, 1958, **28**, 258.
57. J. W. Cahn and J. E. Hilliard, *J. Chem. Phys.*, 1959, **31**, 688.
58. H. Liu, Y. Zhang and A. J. Valocchi, *J. Comput. Phys.*, 2012, **231**, 4433–4453.
59. M. Ahmadiouydarab, Z.-S. (Simon) Liu and J. J. Feng, *Int. J. Multiph. Flow*, 2012, **47**, 85–93.
60. R. G. Cox, *J. Fluid Mech.*, 2006, **168**, 169.
61. O. V. Voinov, *Fluid Dynam.*, 1976, **11**, 714–721.

62. R. Hunter, *Zeta potential in colloid science : principles and applications*, Academic Press, London ;New York, 1981.
63. S. S. Bahga, O. I. Vinogradova and M. Z. Bazant, *J. Fluid Mech.*, 2010, **644**, 245.
64. T. Qian, X.-P. Wang and P. Sheng, *J. Fluid Mech.*, 2006, **564**, 333.
65. T. Qian, X.-P. Wang and P. Sheng, *Phys. Rev. E*, 2003, **68**, 016306.
66. P. Yue, C. Zhou and J. J. Feng, *J. Fluid Mech.*, 2010, **645**, 279.